Nonsequential double ionization of the hydrogen molecule: Dependence on molecular alignment

S. Baier and A. Becker
Max-Planck-Institut für Physik komplexer Systeme, Nöthnitzer Straße 38, D-01187 Dresden, Germany

L. Plaja
Departamento de Física Aplicada, Universidad de Salamanca, E-37008 Salamanca, Spain
(Received 11 March 2008; revised manuscript received 21 May 2008; published 14 July 2008)

We present and analyze results of *ab initio* computations of nonsequential double ionization of the hydrogen molecule in a few-cycle intense laser pulse. To this end, we have used a model of planar molecules with static nuclei, in which the electronic center-of-mass motion is restricted along the polarization direction of the linearly polarized laser. Alignment of the internuclear axis parallel and perpendicular to the polarization axis of the laser field are considered. We show how the relative electron dynamics, parallel and transversal to the field polarization axis, can be used to resolve the different pathways to nonsequential double ionization. Besides the well-known mechanisms, namely, simultaneous emission of an electron pair upon rescattering and recollision-induced excitation with subsequent field ionization, we identify two additional pathways. According to our interpretation the latter are due to a decay of doubly excited states, created during the recollision event, and correlated electron emission after soft recollision. Finally, we analyze the relative strengths of the different contributions to nonsequential double ionization as a function of the laser intensity.

DOI: 10.1103/PhysRevA.78.013409 PACS number(s): 33.80.Rv, 42.50.Hz

I. INTRODUCTION

Due to the technological progress in the generation of ultrafast laser pulses the interaction of atoms and molecules with such intense light sources has gained much attention in recent years. One of the basic issues in this respect is the dynamical role of electron correlations in an atom or molecule exposed to the external field. The correlations become most apparent in double and multiple ionization of neutral atoms or molecules at near-infrared wavelengths (e.g., at the Ti:sapphire wavelengths around 800 nm) and peak intensities of 10^{13}–10^{15} W/cm^2. Experimental data of the yields of doubly and multiply charged ions are found to exceed by many orders of magnitude the theoretical predictions of a stepwise and uncorrelated ionization of one electron after the other by the field (e.g., [1–5]). The observations therefore implied the breakdown of a single-active-electron assumption and exhibit the importance of electron correlation for this so-called nonsequential double (multiple) ionization (NSDI) process (for a recent review, see e.g., [6]).

It is nowadays widely accepted that the correlated emission of electrons from the atom or molecule is due to the so-called recollision process (previously also named antenna process [7,8]). According to this interpretation at first, one electron gets active by the interaction with the field and is emitted from the atom or molecule via tunnel ionization through the combined barrier of the Coulomb potential and the external field. The electron is then driven by the oscillating field first away from and then back to the parent ion. The recollision of the electron with the ion is the common origin of different pathways leading to the emission of a second (or even more) electron(s). Originally, a simultaneous emission (SE) of both electrons initiated by the recollision of the first electron has been considered. Later, an additional pathway has been proposed [9–12], in which the recolliding electron first excites the ion and the external field then ionizes the excited ion at a later time in the pulse. The latter mechanism is nowadays also termed as recollision-induced excitation with subsequent field ionization (RESI).

As mentioned above, NSDI has been observed in atoms as well as in molecules [2,13–16]. While the basic rescattering mechanisms appear to be present independently of the target structure, it is rather unknown how molecular features, such as orbital symmetries, many-center interference effects, orientation of the molecule or vibrations, do influence the NSDI process. First insights regarding the alignment dependence are provided by recent experiments on NSDI in N_2 and O_2 [17,18]. Among others it has been observed that the relative strength of the two pathways (SE and RESI) depend on the alignment of the molecule with respect to the polarization direction [17].

Theoretical analysis of the NSDI process is a challenging task, as the corresponding two-electron Schrödinger equation is a 6+1-dimensional partial differential equation in space and time. Theoretical developments regarding the two-electron atomic problem include the *ab initio* numerical solution of the Schrödinger equation in full [19–21] and reduced dimensions [22–27], *S*-matrix calculations [10,28–33], classical trajectory Monte Carlo calculations [34], and classical Wannier-type calculations [35,36]. For a more detailed review of the theories of NSDI we refer to [37].

Some of these theoretical methods have been extended to the molecular case. In classical calculations the decay of a highly excited two-electron molecule, formed after rescattering, has been analyzed by identifying the saddles of the effective adiabatic potential energy surface. The results did not show significant signatures of the alignment of the molecule on the momentum distribution of the two electrons [38]. On the other hand, an extension of the semiclassical quasistatic model did show an alignment effect of the double-to-single ionization ratio [39–41]. In this model the motion of a two-electron system, created by tunneling of the first electron considering the two-center characteristics of a diatomic molecule, is determined by the classical Newton equations. Nu-

merical simulations in reduced dimensions with static [42,43] and moving nuclei [44] have been performed up to now for alignment of the hydrogen molecule along the polarization axis only.

Below, we will present and compare results of *ab initio* calculations for alignment of the molecule parallel and perpendicular to the field direction. To this end, we make use of a recently introduced approximation of the two-electron problem, in which the center-of-mass motion of the two electrons is restricted to one dimension along the polarization axis of the laser field, whereas the relative electron motion is kept unchanged [26,42,43]. Previously, we were able to identify the SE and RESI mechanisms of double ionization of the hydrogen molecule aligned along the polarization direction [42,43]. Based on the same approximation, we now introduce a planar two-electron diatomic model, which allows us to consider different alignments of the molecular axis with respect to the laser polarization direction. The paper is organized as follows: In Sec. II we introduce and characterize the planar two-electron model of the hydrogen molecule. Next, in Sec. III A we present snapshots of numerical simulations for the parallel and perpendicular alignment of the molecule. The results will be used to identify the different pathways to NSDI of the molecule via the relative electron dynamics parallel and transversal to the polarization direction. Based on this analysis we then quantify the different mechanisms contributing to NSDI and compare their relative strengths for the two alignments in Sec. III B. Finally, conclusions are given in Sec. IV.

II. H_2 MODEL BEYOND ONE-DIMENSIONAL APPROXIMATION

In this section we sketch a recently introduced two-electron model for atoms [26] and aligned molecules interacting with an intense linearly polarized laser field [42,43], which treats the correlated electron motion beyond the traditional one-dimensional approximation (e.g., [45–47]). The key approximation of the model is to consider the center-of-mass motion as one dimensional along the laser polarization axis, while retaining the relative electron dynamics in its full complexity. In the present study, the introduction of molecular alignment as a degree of freedom forces us to consider planar molecules to reduce the computational load. We should stress that the dimensional reduction of the center-of-mass motion is only compatible with molecular geometries symmetric with respect to the polarization axis, i.e., axial and perpendicular alignments. In the following we will characterize the features of the approximations through the comparison of the relevant states and energies of the H_2 and H_2^+ molecules for the NSDI process in the cylindrical, planar, and perpendicular cases.

A. Cylindrical and planar H_2 models

The Hamiltonian of a hydrogen molecule with frozen nuclei interacting with a linearly polarized intense laser pulse can be written in dipole approximation as (Hartree atomic units, $e=m=\hbar=1$, are used)

$$H=\frac{\mathbf{P}^2}{4}+\mathbf{p}^2-\frac{\mathbf{P}\cdot\mathbf{A}(t)}{c}+\frac{1}{r}-\frac{2}{|2\mathbf{R}+\mathbf{R}_k+\mathbf{r}|}-\frac{2}{|2\mathbf{R}+\mathbf{R}_k-\mathbf{r}|}-\frac{2}{|2\mathbf{R}-\mathbf{R}_k+\mathbf{r}|}-\frac{2}{|2\mathbf{R}-\mathbf{R}_k-\mathbf{r}|}, \quad (1)$$

where $\mathbf{R}=(\mathbf{r}_1+\mathbf{r}_2)/2$, $\mathbf{P}=\mathbf{p}_1+\mathbf{p}_2$, $\mathbf{r}=\mathbf{r}_1-\mathbf{r}_2$, and $\mathbf{p}=(\mathbf{p}_1-\mathbf{p}_2)/2$ are the center-of-mass and relative coordinates and momenta of the two electrons, respectively. $\pm\mathbf{R}_k/2$ denotes the positions of the two nuclei with respect to the origin of the coordinate system, which is chosen to correspond with the center-of-mass of the nuclei. $\mathbf{A}(t)$ is the vector potential of the linearly polarized field. In the representation of the two-electron Hamiltonian in the center-of-mass and relative coordinates, the two primary interactions for the double ionization process, namely, the electron-field interaction and the electron-electron interaction are decoupled. While the vector potential couples to the center-of-mass coordinate of the two electrons, the electron repulsion is connected to the relative coordinate only.

A solution of the time-dependent Schrödinger equation corresponding to the full Hamiltonian, Eq. (1), requires the integration of a partial differential equation with six dimensions in space and one in time. This is at the limit of present supercomputer systems for studies at experimental laser parameters, i.e., Ti:sapphire frequencies and intensities of more than 10^{14} W/cm^2. A feasible strategy to reduce the computational effort is to consider models in which the degrees of freedom in the two-electron system are reduced. For the case of a linearly polarized field, the most recurrent approximation is to reduce the system dimensionality to two, one for each electron, plus time (e.g., [45–47]). This kind of approximation has been applied successfully to single-active-electron effects, such as single ionization and sequential double ionization, where the interaction of individual electron(s) with the linearly polarized field plays the dominant role. However, as pointed out at the outset, in nonsequential double ionization the electron-electron repulsion becomes a relevant interaction too. In contrast to the electron-field interaction, in this case the corresponding term, $1/r$ in Eq. (1), does not have a preferred directionality and, therefore, the reduction to one dimension per electron is not desirable.

In order to improve the 1D description we have recently proposed an alternative model [26,42,43] that restricts the center-of-mass motion of the two electrons to one dimension along the polarization direction, but leaves the relative motion unrestricted. For molecules aligned with the field polarization, the combination of this approximation with the cylindrical symmetry reduces the complexity of the problem to three dimensions: one for the center-of-mass (Z) and two for the relative coordinate (ρ, perpendicular, and z, parallel to the field polarization), as depicted in Fig. 1(a).

In the general case of arbitrarily aligned molecules due to the absence of a particular symmetry the dimensional reduction of the center-of-mass coordinate would simplify the problem from six to four dimensions only. In order to tackle effectively the alignment problem, a further dimensional reduction is required. Our choice has been to consider an initial problem of planar H_2 molecules (i.e., two electrons evolving

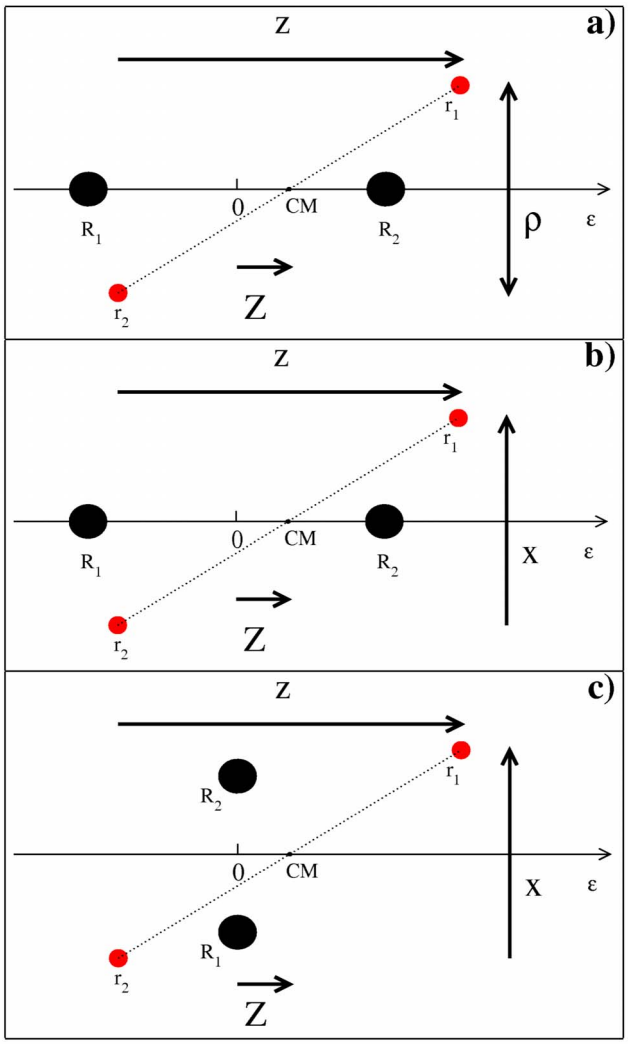

FIG. 1. (Color online) Illustration of the coordinate systems: $\mathbf{R}_1$ and $\mathbf{R}_2$ denote the positions of the nuclei located symmetrically about the center of the coordinate system and aligned parallel [panels (a) and (b)] and perpendicular [panel (c)] to the polarization axis ϵ, respectively. $\mathbf{r}_1$ and $\mathbf{r}_2$ denote the positions of the electrons. The center-of-mass coordinate of the electrons is restricted to the polarization axis. In panels (b) and (c) the relative coordinate r is restricted to a plane spanned by z and x.

in a two-dimensional space each). In this case the four dimensions of the general problem are reduced to three as the center-of-mass is restricted to the polarization axis. The corresponding three-dimensional model Hamiltonian is given by

$$H_{planar} = \frac{P_z^2}{4} + p_x^2 + p_z^2 - \frac{P_z A(t)}{c} + \frac{1}{\sqrt{x^2+z^2}} + V_{en}(\Theta), \quad (2)$$

with the Coulomb potential between the electrons and the nuclei

$$V_{en}(\Theta) = -\frac{1}{\sqrt{\left(Z+\frac{z}{2}+\frac{R_k\cos\Theta}{2}\right)^2+\frac{(x+R_k\sin\Theta)^2}{4}+a_{planar}^2}} - \frac{1}{\sqrt{\left(Z-\frac{z}{2}+\frac{R_k\cos\Theta}{2}\right)^2+\frac{(x-R_k\sin\Theta)^2}{4}+a_{planar}^2}} - \frac{1}{\sqrt{\left(Z+\frac{z}{2}-\frac{R_k\cos\Theta}{2}\right)^2+\frac{(x-R_k\sin\Theta)^2}{4}+a_{planar}^2}} - \frac{1}{\sqrt{\left(Z-\frac{z}{2}-\frac{R_k\cos\Theta}{2}\right)^2+\frac{(x+R_k\sin\Theta)^2}{4}+a_{planar}^2}}, \quad (3)$$

where Θ is the inclination angle between the internuclear axis and the polarization axis and a_{planar}^2 is a parameter to soften the Coulomb potential. In the following we will consider the two special cases of alignment of the internuclear axis parallel ($\Theta=0$) and perpendicular ($\Theta=\pi/2$) with respect to the polarization axis. The corresponding coordinate systems for these two configurations are illustrated in Figs. 1(b) and 1(c). Again, Z represents the center-of-mass coordinate of the two electrons, which is restricted to the polarization direction. z and x denote the relative coordinates of the two electrons parallel and perpendicular to the polarization axis, respectively. Please note that the cylindrical H_2 model for molecules aligned along the polarization axis, which has been studied by us before [42,43], is given by replacing x by ρ and setting $\Theta=0$ in Eqs. (2) and (3). In addition, the soft Coulomb parameter differs in the planar (a_{planar}^2) and cylindrical (a_{cyl}^2) models.

B. Eigenstates and energies

Before we proceed with the numerical calculations for the double ionization dynamics, it seems necessary to characterize the degree of accuracy retained in assuming the planar molecule approximation, as well as the coherence between our molecular models after the dimensional reduction of the center-of-mass coordinate for different molecular alignments. In particular, for the study of nonsequential double ionization, we should focus our attention on the consistence of the ionization potential of H_2, the excitation energies of H_2^+, and the eigenstate geometries for the planar model in the two alignments and the cylindrical (parallel alignment) model.

The ground and excited states of H_2 and H_2^+ are obtained via imaginary time propagation of an initial guess wave function. In case of the excited states the energetically lower states are projected out at every time step. For simplicity, we have calculated the states for H_2^+ using the same code as in the case of H_2, but dropping the electron-electron interaction term in the Hamiltonians in Eq. (2). This corresponds to an independent particle model. The resulting energies are rescaled to obtain the quantities for a single electron.

In the calculations we have fixed the nuclei at $R_k=1.4$ a.u., which corresponds to the literature value for the equilibrium distance of H_2. The parameters $a_{cyl}^2=0.366$ in the cylindrical configuration (cf. [42]) and $a_{planar}^2=0.622$ in the

TABLE I. Energies of the two lowest eigenstates of H_2 and H_2^+ in the current model configurations, calculated via imaginary time propagation of the time-dependent Schrödinger equation. We have used R_k=1.4 for all configurations, a_{cyl}^2=0.366 for the cylindrical configuration, and a_{planar}^2=0.622 for both planar configurations.

Configuration	State	H_2	H_2^+
Cylindrical	E_0	−1.1741	−0.5605
	E_1	−0.8290	−0.2635
Parallel	E_0	−1.1745	−0.6257
	E_1	−0.9450	−0.3392
Perpendicular	E_0	−1.1297	−0.5809
	E_1	−0.8307	−0.2755

planar one are chosen such that the respective ground state energies of H_2 for the parallel configurations are close to the literature value in Born-Oppenheimer approximation [48]. Table I shows the energies of the two lowest eigenstates of H_2 and H_2^+ in the three configurations. The eigenvalues of the states differ for the different models due to the restriction of the motion of the two electrons. The restriction of the center-of-mass coordinate along the polarization direction, for example, inhibits contributions from ionic configurations in the case of perpendicular alignment but not for parallel alignment. Note that the single ionization potentials $[E_0(H_2)-E_0(H_2^+)]$ in the planar parallel and perpendicular configurations are almost equal (difference below 10^{-4} a.u.), while the energy differences between the ground and the first excited states of H_2^+ are slightly larger in the perpendicular configuration ($|E_1(H_2^+)-E_0(H_2^+)|$=0.2951 a.u.) than in the parallel alignment ($|E_1(H_2^+)-E_0(H_2^+)|$=0.2827 a.u.).

Next, we present in Figs. 2 and 3 the spatial probability distributions of those states of H_2 and H_2^+, which will be relevant for the analysis of the numerical calculations below. We show the results obtained for the three configurations, cylindrical (upper panels), planar with parallel alignment (middle panels), and planar with perpendicular alignment of the molecular axis (lower panels), integrated over the perpendicular component of the relative coordinate, x and ρ, respectively, in the panels of the left-hand columns, and integrated over the parallel component of the relative coordinate z in the panels of the right-hand columns.

The ground state of H_2 (Fig. 2) exhibits the expected pronounced covalent nature with two maxima in the z-Z distribution for both the parallel [panels (a) and (c)] and in the x −Z distribution for the perpendicular alignment [panel (f)], respectively. In the cylindrical configuration the two maxima are closer to each other.

Figure 3 shows the distributions corresponding to the first two excited states of the two-electron H_2^+. As explained above, the results are obtained using the Hamiltonian for H_2 but dropping the electron-electron interaction term. The present distributions in this independent particle presentation correspond to the overlap of two one-electron states. The ground state (not shown) represents an overlap of two electrons in the $1s\sigma_g$ orbital. The first excited state within the two-electron model is the overlap of one electron in the $1s\sigma_g$ orbital and one in the $2p\sigma_u$ orbital. This state is twofold

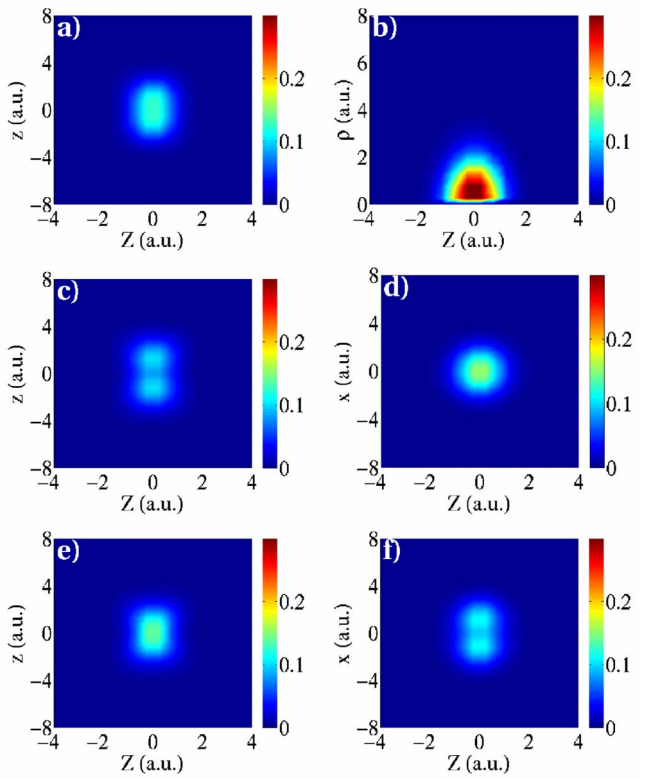

FIG. 2. (Color online) Ground state probability densities of H_2 for the three model configurations: cylindrical (upper panels), planar parallel (middle panels), and planar perpendicular (lower panels). Left-hand column: Densities integrated over the relative coordinate perpendicular to the polarization axis, x and ρ, respectively. Right-hand column: Densities integrated over the relative coordinate along the polarization axis z.

degenerated. The respective probability densities are shown in Fig. 3. The two columns on the left represent one and those on the right the other state, respectively. Please note, that between the parallel and the perpendicular alignments the two states are interchanged. The averaged energy value of the two states, E_1, is given in Table I. Figures 2 and 3 show that the relevant states of H_2 and H_2^+ are accurately modeled within the cylindrical model as well as within the planar model.

These obtained probability densities may impact our quantitative studies on the alignment dependence of nonsequential double ionization as follows. On one hand, we may expect similar single ionization probabilities for both alignments, as the ionization potentials of H_2 are identical in both model configurations and ionization from a σ_g orbital is expected to be rather independent of the molecular alignment [49–51]. Rescattering can either lead to simultaneous emission of the two electrons [7,8] or to an excitation of the H_2^+ ion, which ionizes at some time later (RESI) [9–12]. Simultaneous emission occurs due to single ionization followed by a laser-assisted electron-impact ionization. In view of the almost identical single ionization potentials, the difference in the double ionization potential should, but weakly, affect the probabilities for electron-impact ionization. We, however, expect that this does not influence the conclusions of the

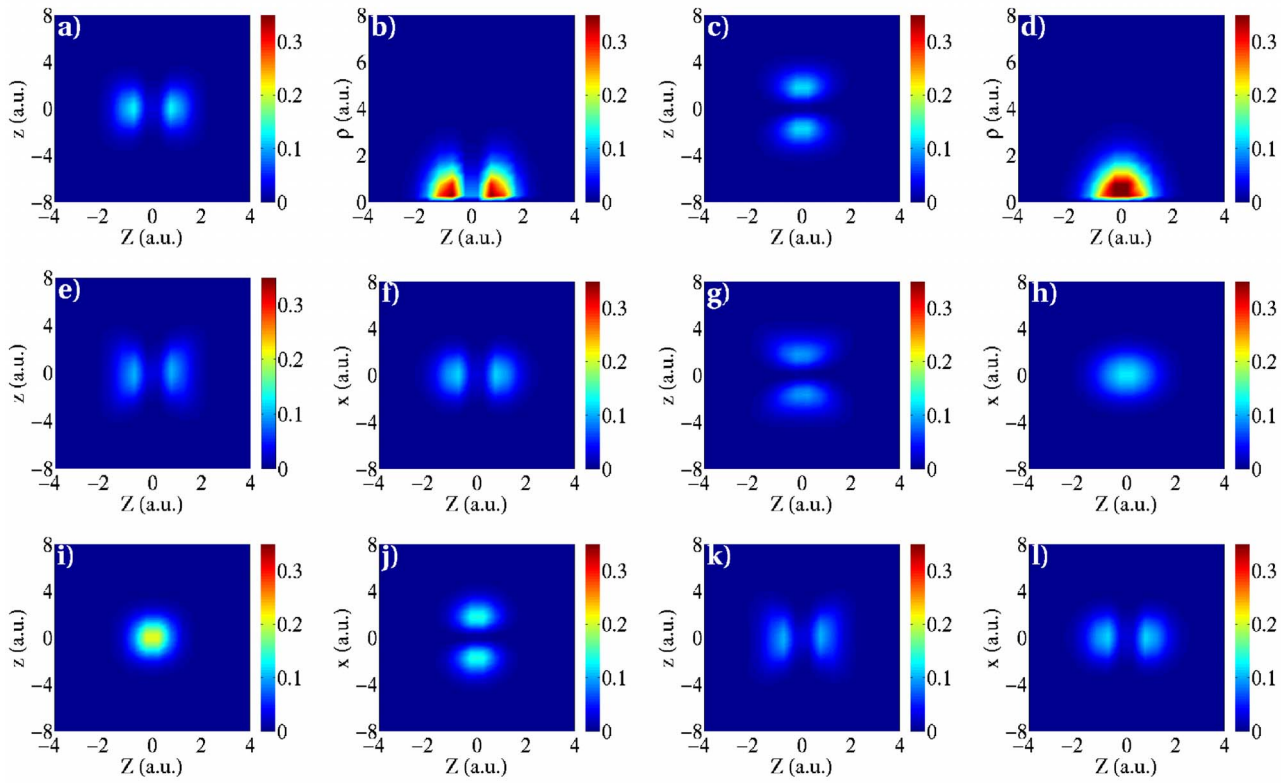

FIG. 3. (Color online) Probability densities of the first two excited states of the two-electron H_2^+ model system for the three configurations: cylindrical (upper panels), planar parallel (middle panels), and planar perpendicular (lower panels). First and third column: Densities integrated over the relative coordinate perpendicular to the polarization axis, x and ρ, respectively. Second and fourth column: Densities integrated over the relative coordinate along the polarization axis z.

present manuscript. On the other hand, for the RESI process one has to consider that ionization from (excited) σ_u states is found to be more efficient in parallel alignment [49].

III. NONSEQUENTIAL DOUBLE IONIZATION FOR DIFFERENT MOLECULAR ALIGNMENTS

In this section we present the results of numerical simulations for double ionization using the planar model for alignment of the molecular axis parallel and perpendicular with respect to the polarization axis. We will also compare the different pathways leading to double ionization with those identified by using the cylindrical model for the aligned molecule [42]. To draw conclusions of the quantitative differences we will then introduce an approximative method to distinguish the different pathways.

For the simulations we have solved the time-dependent Schrödinger equations using the Crank-Nicholson method on a grid. The parameters of the grid for the cylindrical and the planar models have been chosen as $\Delta\rho=\Delta z=\Delta x=\Delta Z=0.5$ a.u. and the time step was $\Delta t=0.025$ a.u. The grid extended over 300 grid points in the x (150 in ρ) direction, 500 points in the z direction, and 250 points in the Z direction. $\cos^{1/2}$-like absorbing mask functions have been used to avoid reflections at the boundaries. The grid parameters incur a momentum resolution of less than 0.050 a.u. and a maximal momentum of 6.3 a.u. within the planar model, which is sufficient for the present calculations.

In order to analyze the results with respect to single and double ionization we have partitioned the coordinate space as follows [42]:

H_2 molecule: $r_1 < 17.3$ a.u. and $r_2 < 17.3$ a.u.
H_2^+ ion: either $r_1 < 14.0$ a.u. and $r_2 > 17.3$ a.u.
or $r_1 > 17.3$ a.u. and $r_2 < 14.0$ a.u.
H_2^{2+} ion: complementary space,

with r_1 and r_2 being the moduli of the vector positions of the two electrons ($r_{1,2}=\sqrt{(Z\pm\frac{z}{2})^2+\frac{x^2}{4}}$ in case of the planar model and $r_{1,2}=\sqrt{(Z\pm\frac{z}{2})^2+\frac{\rho^2}{4}}$ for the cylindrical model). In Fig. 4 the partition of the grid is exemplified for the planes $z=0$ (left-hand panel) and $x=0$ (right-hand panel). Population in the brown (bound) and blue region (SI) will be identified as H_2 and H_2^+ contributions, respectively. The complementary space contains the doubly ionized part. The geometrical configuration of the electron pair in the DI region is sketched in the right-hand panel: probability densities located in the upper and lower triangles correspond to the location of electrons at opposite sides of the nuclei, and those located in the left and right triangles correspond to locations of the electrons at the same side. The boundaries are chosen such that the probability densities of the H_2 model system are decreased by more than 13 orders of magnitude with respect to the maximum of the corresponding bound state. Test calcu-

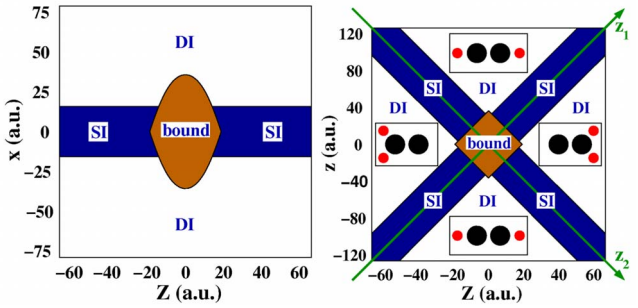

FIG. 4. (Color online) Partition of the grid transversal to ($z=0$) (left-hand panel) and in ($x=0$) the polarization plane (right-hand panel). Acronyms denote the regions of the neutral molecules (bound), single (SI), and double ionization (DI). In the right-hand panel also sketched are the locations of the electrons (red, small circles) with respect to the nuclei (black, large circles) in the different DI regions.

lations with different boundaries have shown that the results qualitatively do not depend on the particular choice of the boundaries.

We compare the double ionization dynamics for the two alignments of the molecular axis in the planar model (as well as in the cylindrical model) by considering the interaction with a seven-cycle linearly polarized ramp pulse (two cycles turn on and two cycles switch off) with a carrier frequency of $\omega=0.057$ a.u., equivalent to a wavelength of 800 nm. The DI densities plotted in the following will correspond to integration of the probabilities over z and x, respectively.

A. Identification of the double ionization mechanisms

In Fig. 5 we present the single (green, light lines) and double ionization (black, dark lines) probabilities as a function of time along with the electric field of the pulse corresponding to a peak intensity of $I=2\times10^{14}$ W/cm^2 (black dotted line). The general trend of the curves is quite similar. In both models and both alignments the single ionization curves rise shortly after the field maxima in agreement with the field (tunnel) ionization picture. The small dips are due to the return of a part of the single ionized wave packets, which are counted as bound contributions as they cross the nuclei (cf. Fig. 4). As expected from the similarity in the ionization energies (cf. Table I), the ionization probabilities for the two different alignments in the planar model (parallel alignment: solid line; perpendicular alignment: dashed line) are quantitatively very similar. We may, however, note that the ionization probability is slightly larger for perpendicular (0.198) than parallel alignment (0.186) of the molecule. This result does not agree with the experimental observation for alignment-dependent ionization of the N_2 molecule, which has a highest occupied molecular orbital of σ_g symmetry too ([50]). Whether this is due to any difference in the nature of alignment-dependent ionization of H_2 and N_2 or, what seems to be more likely, due to the restriction of the center-of-mass coordinate in the present model, is at present unclear.

On the other hand, the single and double ionization probabilities are significantly larger than those obtained in the

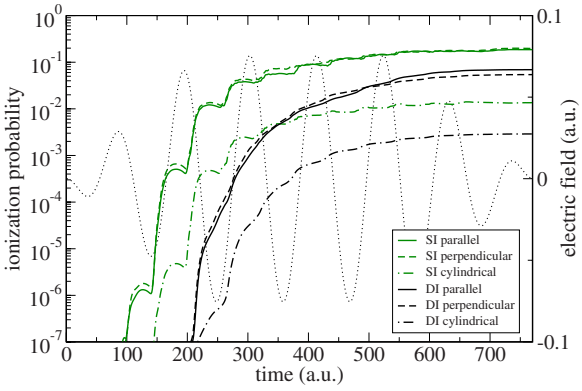

FIG. 5. (Color online) Single (green, light lines) and double ionization probabilities (black, dark lines) as a function of time. A comparison between the predictions of the planar model for parallel (solid lines) and perpendicular (dashed lines) alignment of the molecule and those of the cylindrical model (dashed-dotted lines) is shown. The amplitude of the laser field is displayed by the black dotted line. The intensity of the laser pulse is $I=2\times10^{14}$ W/cm^2.

cylindrical model (dashed-dotted lines; 0.014 for single ionization and 0.0029 for double ionization). This difference is probably due to the restriction of the electron motion to two dimensions in the planar model, which effectively enhances the electron-field interaction and, hence, results in higher ionization probabilities than in the cylindrical model. The double ionization curves have steep rises around the zeros of the field, which is a typical signature of the simultaneous double electron emission upon rescattering. However, the DI probabilities also increase during the field maxima, at which mechanisms like the RESI process are expected to occur. We note that the ratio between single and double ionization is smaller (between 2.7 and 4.7) in the three models as compared to experimental results [52]. In our opinion, this should be attributed to the reduction of the center-of-mass motion of the two electrons, which intrinsically enhances the electron-electron interaction.

In order to distinguish different paths to NSDI, we show snapshots of DI probability densities at several instants of time during one rescattering event. From the snapshots we can identify the wave packets as they appear in the DI regions, and analyze especially their subsequent evolution in the components of the relative coordinate of the two electrons, which is dominated by the electron-electron correlation.

At first, we present in Fig. 6 snapshots taken at $t=424$ a.u. The results are obtained using the planar model for alignment of the molecular axis parallel (left column) and perpendicular (right column) with respect to the polarization axis. Snapshots in the upper row correspond to DI densities integrated over the relative coordinate along the polarization direction z, while those in the lower row are integrated over the transversal component x. Please note that the horizontal axis in each snapshot represents the center-of-mass coordinate Z. We identify four different pathways to NSDI (labeled with 1.–4. in Fig. 6), which we attribute as the well-known simultaneous emission of an electron pair upon rescattering (1.), the RESI process (2.), and two additional mechanisms,

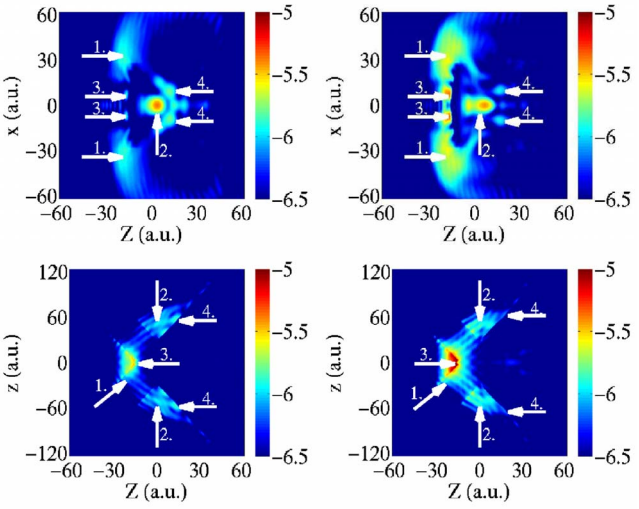

FIG. 6. (Color online) DI probability densities taken at $t=424$ a.u. for parallel alignment (left column) and perpendicular alignment (right column) of the molecule. The distributions are integrated over z (upper row) and x (lower row), respectively. Arrows with different labels indicate the contributions corresponding to different NSDI mechanisms (1.: Simultaneous emission upon rescattering, 2.: Recollision-excitation with subsequent field ionization, 3.: Decay of recollision-induced doubly excited states, and 4.: Correlates emission after soft collision).

which we interpret as the decay of doubly excited states (3.) and a correlated emission after soft recollision events (4.). Each of these mechanisms appears to be present for both alignments of the molecule. Despite differences in their relative strength, which will be discussed in Sec. III B, we note that each contribution appears slightly later in time in case of perpendicular alignment of the molecular axis as compared to the case of parallel alignment. The qualitative behavior of all DI contributions is similar for both considered molecular alignments. Therefore, we only examine the perpendicular molecular alignment in the following analysis of the temporal evolution of the DI mechanisms.

Before proceeding in discussing the different pathways, we note that each of them appears due to a single recollision event. In order to draw this conclusion we have performed additional test calculations, in which we have absorbed the outgoing single ionized wave packet, corresponding to the present rescattering event (for technical details cf. [42]). This suppression of the return of the wave packet to the ion is found to result in a disappearance of all contributions to DI, discussed below.

1. Simultaneous emission (SE) upon rescattering

The simultaneous emission (SE) of the electron pair occurs immediately after the first electron scatters with the molecular ion. It is particularly relevant at times when the field vanishes (i.e., when the most energetic rescattering takes place). We have identified this mechanism already before in the numerical simulations using the cylindrical model [42,43]. The emission of the second electron is a result of the impact of the first, while the electromagnetic field plays a secondary role. The picture associated with this pathway is an emission of both electrons primarily to the same side of the nuclei; the relative distance between the electrons transversal to the polarization direction increases quickly in time due to the strong Coulomb repulsion.

The temporal evolution of this process can be seen in Fig. 7, where this part is marked with white arrows. The DI densities are shown for $t=378$ a.u. (first column), $t=388$ a.u. (second column, near field zero), $t=398$ a.u. (third column), and $t=418$ a.u. (fourth column). The doubly ionized wave packet appears in the right triangle of the $Z-z$ distributions (snapshots in the lower row). It is driven by the field in the negative Z direction. As expected, during this evolution the transversal relative distance x between the two electrons quickly grows (snapshots in the upper row).

2. Recollision-excitation with subsequent field ionization (RESI)

The so-called RESI mechanism is a NSDI process, in which the recollision of the first electron is not energetic

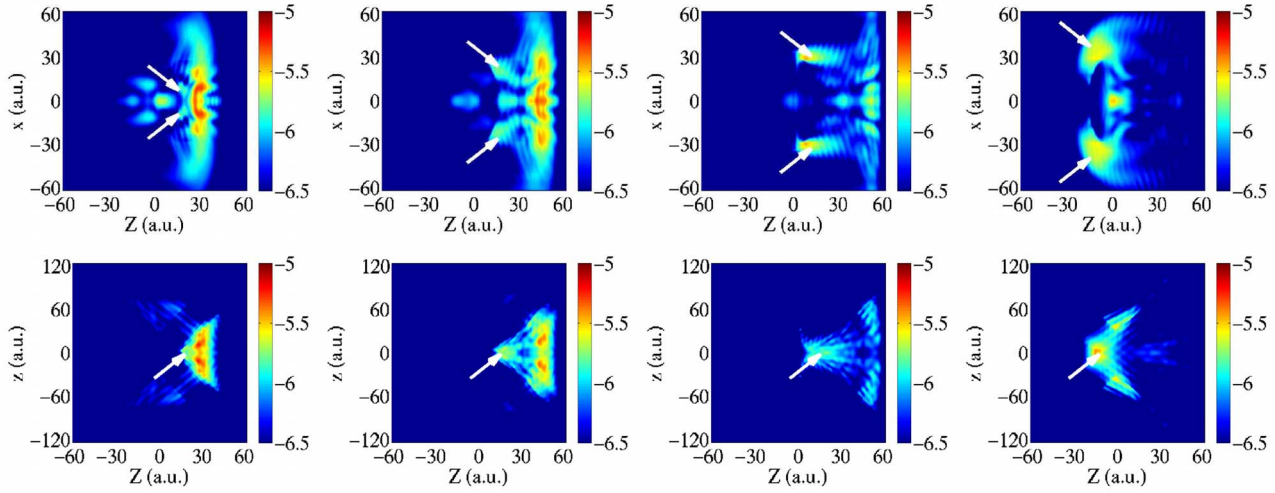

FIG. 7. (Color online) Integrated DI probability densities taken at $t=378$ a.u. (first column), $t=388$ a.u. (second column), $t=398$ a.u. (third column), and $t=418$ a.u. (fourth column) for perpendicular alignment. The distributions are integrated over z in the upper and over x in the lower row. The arrows indicate the contributions corresponding to simultaneous emission upon rescattering.

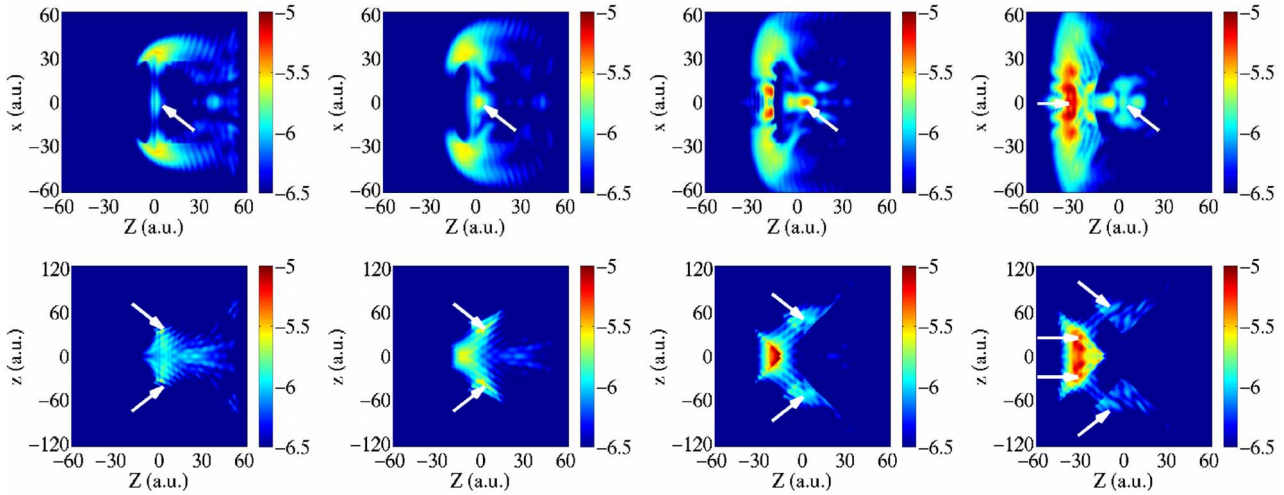

FIG. 8. (Color online) Same as Fig. 7, but the densities are taken at $t=405$ a.u. (first column), $t=415$ a.u. (second column), $t=425$ a.u. (third column), and $t=435$ a.u. (fourth column). The arrows indicate the contributions corresponding to recollision excitation with subsequent field ionization.

enough to release the second electron from the molecular ion, but the latter is promoted into an excited state. The double ionization process happens at a later time through the interaction of the electron in the excited state with the rising field. Figure 8 shows the RESI contributions. The snapshots are taken at $t=405$ a.u. (first column), $t=415$ a.u. (second column), $t=425$ a.u. (third column), and $t=435$ a.u. (fourth column). The respective DI wave packets are released around the field maximum ($t=413$ a.u.) from the SI region, indicating field ionization out of the states of the singly ionized hydrogen molecular ion (cf. $Z-z$ distributions in the lower row). It has been shown before [42,43] that such contributions arise predominantly from the excited states populated via the recollision process, as expected for the RESI process. The kinematics of the doubly ionized wave packet are such that the electrons are ejected at opposite sides of the molecule (upper and lower triangles of the $Z-z$ distributions). Therefore, the correlation between the electrons is small, which leads to almost negligible dynamics of the electrons perpendicular to the polarization direction, as it can be seen from the $Z-x$ distributions. Please note, that parts of the RESI contribution are driven by the field through the singly ionized and bound regions before they appear in the left triangle of the $Z-z$ distribution (right column).

3. Decay of recollision-induced doubly excited states (DRIDES)

Besides these two mechanisms we can clearly identify two further DI contributions in the snapshots in Fig. 6. One of the contributions is marked with 3 and its temporal evolution is shown in Fig. 9, where the snapshots are taken at $t=425$ a.u. (first column), $t=430$ a.u. (second column), $t=435$ a.u. (third column), and $t=445$ a.u. (fourth column). These wave packets are released from the bound region into the left triangle of the $Z-z$ distributions. There they partially

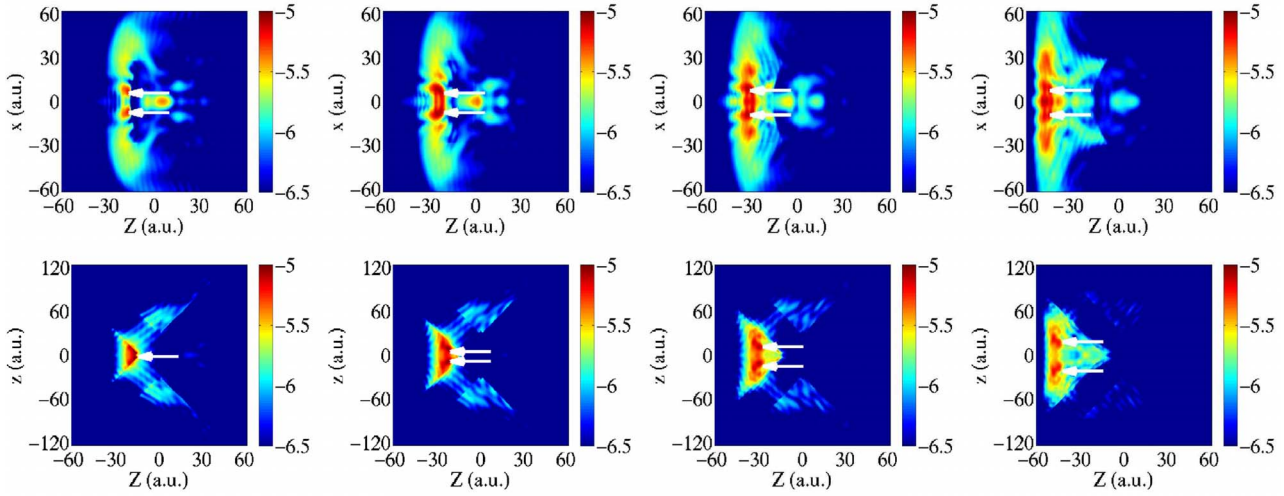

FIG. 9. (Color online) Same as Fig. 7, but the densities are taken at $t=425$ a.u. (first column), $t=430$ a.u. (second column), $t=435$ a.u. (third column), and $t=445$ a.u. (fourth column). The arrows indicate the contributions corresponding to the decay of recollision-induced doubly excited states.

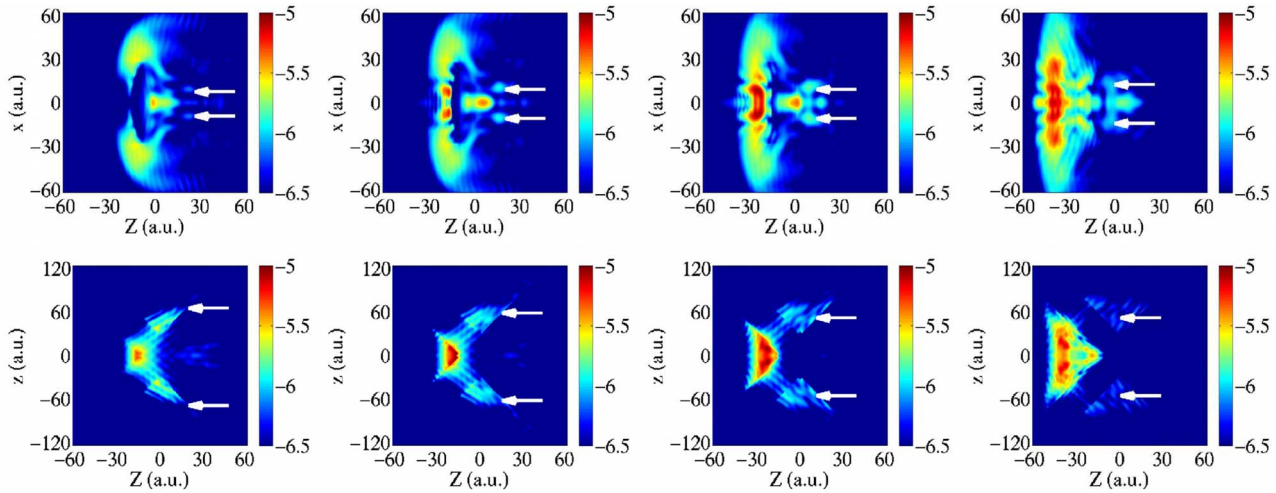

FIG. 10. (Color online) Same as Fig. 7, but the densities are taken at $t=420$ a.u. (first column), $t=425$ a.u. (second column), $t=430$ a.u. (third column), and $t=440$ a.u. (fourth column). The arrows indicate the contributions corresponding to the correlated emission after soft collision.

overlap with the SE contributions and are therefore difficult to identify, in particular, in the previous 1D models. In our case, however, they can be clearly distinguished from other contributions through the probability density along the perpendicular relative coordinate. In the subsequent temporal evolution the relative distances (z and x) between the two electrons slightly increase but much slower as compared to the SE contributions. This agrees with the emission of a weakly correlated two-electron wave packet from the molecule. The rather long time delay between the recollision event and the creation of this correlated DI contribution suggests that the incoming electron leaves its energy entirely to compound a two-electron excited state, which is finally detached from the molecule after the subsequent field maximum. From the comparison (see Fig. 6) it becomes apparent that this process is more probable in the perpendicular configuration, in which the pathway to the double ionization is the same for both the two electrons, while in the parallel case one of the electrons is forced to cross the two potential wells.

4. Correlated emission after soft collision (CESC)

Also taking place after the field maximum, we can identify another NSDI process that is characterized by an almost constant and small relative distance in the perpendicular direction (x) but large axial distance (z). It is marked with 4. in Fig. 6 and the evolution of its wave packets can be seen in Fig. 10. The considered points in time are $t=420$ a.u. (first column), $t=425$ a.u. (second column), $t=430$ a.u. (third column), and $t=440$ a.u. (fourth column). It can be seen that the marked contributions correspond to electrons emitted on opposite sides of the nuclei. In terms of the axial relative dynamics, this process cannot be resolved, as its associated probability density overlaps with the corresponding contribution to the RESI process considered before. However, our model reveals the difference as it shows that the relative distance between the electrons in the perpendicular direction is not zero, as in the case of RESI. This, in fact, shows the correlated origin of the wave packet. On the other hand, the large axial coordinate exhibits the asymmetry of the electron pair after the collision: the second electron accesses the ionization region when the first electron is already far from the molecular ion. This is a major difference to the process of simultaneous emission described above. A second difference is the time at which the electron pair appears in the double ionization region: in SE right after the rescattering, i.e., near the zero of the field, while in the present case more than a quarter of a cycle later. These two facts suggest a soft rescattering in which the first electron releases a small part of its energy to promote the second just above the ionization threshold. Afterwards, it slowly drifts toward the spatial region defined for double ionization where it appears at a later time.

B. Relative strengths of the pathways

Next, we will analyze quantitatively the strengths of the different pathways to double ionization for the two molecular alignments considered. As discussed in the last section, the mechanisms differ in the separation of the electrons in the direction perpendicular to polarization axis. While in the SE mechanism the two electrons are strongly correlated and, hence, move quickly apart from each other in that direction, the electrons are minimally correlated in the RESI mechanism and propagate along the polarization axis. The other two mechanisms, namely, correlated emission after soft collision (CESC) and decay of recollision-induced doubly excited states (DRIDES), have almost constant $|x|$ (around 10 a.u.). This provides us with a tool to separate the contributions to the double ionization wave packet in the direction perpendicular to the polarization axis. We have chosen $|x| \leq 6.25$ a.u. as the region counted as RESI and everything in the subspace $|x| \geq 15$ a.u. is defined as SE. The region in between contains the other mechanisms.

Using that separation we are in the position to investigate the temporal evolution of double ionization during the pulse. In Fig. 11 we show the ratio of SE to RESI for the parallel

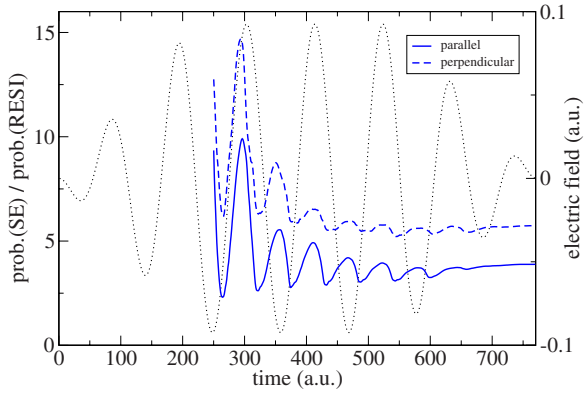

FIG. 11. (Color online) Ratio of DI contributions due to simultaneous emission (SE) to those due to RESI. The dotted black line represents the amplitude of the laser electric field with an intensity of $I=3\times10^{14}$ W cm^{-2}.

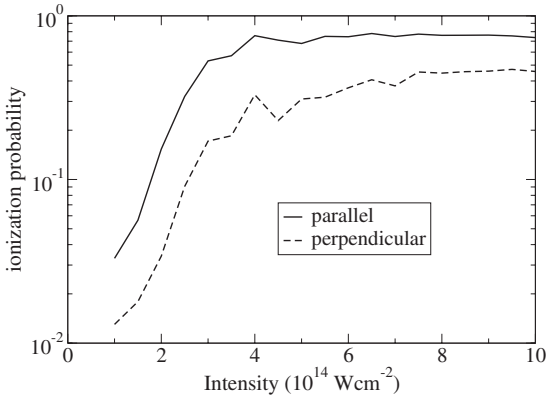

FIG. 13. Comparison of single ionization probabilities from the first excited states (average values) for the parallel (solid line) and perpendicular alignment (dashed line) of the molecule as a function of the intensity.

(solid line) and perpendicular (dashed line) alignments as a function of time. Since the first relevant rescattering event occurs at around $t=220$ a.u., the curves are only plotted for times beyond 250 a.u. The oscillating behavior, with maxima shortly after the zeros of the field and minima shortly after the maxima of the field, reflects the fact that simultaneous emission occurs near the zeros of the field while RESI is most probable at the field maxima. The ratios get constant at a later time due to saturation of ionization. SE exceeds RESI by a factor of 5.7 in perpendicular alignment and 3.9 in parallel alignment.

To draw a conclusion on the relative strengths of these two double ionization mechanisms we look at their dependence on the intensity, shown in Fig. 12. The overall behavior is an almost monotonic rise of all double ionization contributions. Please note that the curves do not show the well-known knee structure, since sequential ionization is suppressed due to absorption of the outgoing single ionized wave packets beyond twice the quiver radius of the electron at the edges of the grid. The contributions from all NSDI mechanisms except RESI are approximately of equal

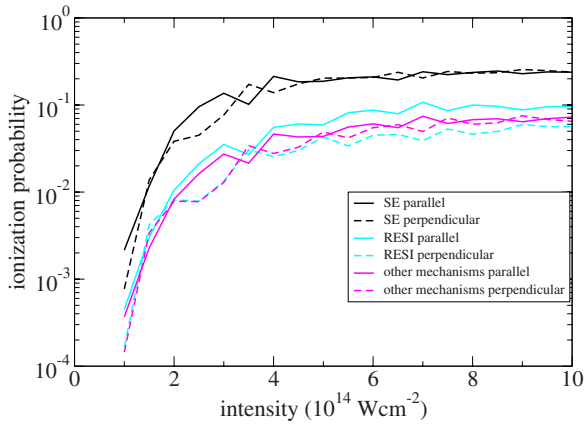

FIG. 12. (Color online) Intensity dependence of simultaneous emission, RESI, and other mechanisms leading to double ionization for the two molecular alignments.

strengths in both alignments. This may be understood as follows: The ionization potential of H_2^+ is a bit smaller for perpendicular configuration which is, however, balanced by the fact that the returning wave packet is slightly wider in the transversal direction for perpendicular alignment, which leads to a less efficient rescattering process. On the other hand, there is a distinct difference for the RESI process. It is significantly stronger in the parallel as compared to the perpendicular alignment of the molecule.

The difference in the probabilities for the RESI process can be readily explained by looking at the ionization probabilities of the two-electron H_2^+ from its first excited states, presented in Fig. 13. Here the averaged value obtained from the two degenerated states is shown. From the results it can be seen that ionization from the first excited state in perpendicular alignment is strongly suppressed. This is in agreement with the results of earlier studies that ionization from a σ_u state [49] is less efficient if the molecule is aligned perpendicular with respect to the polarization axis. Ionization from the second excited state (not shown) has almost the same probability in both configurations, so that the suppression of ionization from the σ_u state qualitatively explains the difference in the RESI probabilities found above.

IV. CONCLUSIONS

We have presented a two-electron model to describe nonsequential double ionization of a hydrogen molecule with fixed nuclei at different alignments of the molecular axis with respect to the polarization axis of the external field. Within the model we restrict the center-of-mass motion of the two electrons to one dimension, parallel to the laser polarization, and the relative motion to a plane containing the molecular and the polarization axes. We have characterized the model and compared our results for single and double ionization with earlier studies. The inclusion of the transversal relative coordinate in our model allows us to resolve the different processes leading to NSDI. In particular, we have shown that the strength of simultaneous emission of a

correlated electron pair upon recollision is quite similar in both alignments, while RESI is more efficient in parallel than perpendicular alignment. This could be explained by the different ionization behavior of the σ_u state of the hydrogen molecular ion in the two alignments. In addition, we have identified two other contributions for NSDI that are characterized by the relative coordinate perpendicular to the laser field. According to our data, we have proposed two ionization mechanisms, namely, the decay of recollision-induced double excited states and the correlated emission after soft collision, that may be responsible for them.

ACKNOWLEDGMENTS

We thank F. He, C. Ruiz, and A. Requate for stimulating discussions. We acknowledge partial support from DAAD (Project No. D/05/25690), MEC (Project No. HA2005-0158, Consolider Program SAUUL, Project No. CSD2007-00013), and GGI-MEC (Project No. FIS2005-01351).

[1] A. L'Huillier, L. A. Lompre, G. Mainfray, and C. Manus, Phys. Rev. Lett. **48**, 1814 (1982).
[2] B. Walker, B. Sheehy, L. F. DiMauro, P. Agostini, K. J. Schafer, and K. C. Kulander, Phys. Rev. Lett. **73**, 1227 (1994).
[3] S. F. L. Larochelle, A. Talebpour, and S. L. Chin, J. Phys. B **31**, 1201 (1998).
[4] C. Cornaggia and P. Hering, J. Phys. B **31**, L503 (1998).
[5] C. Guo, M. Li, J. P. Nibarger, and G. N. Gibson, Phys. Rev. A **58**, R4271 (1998).
[6] A. Becker R. Dörner, and R. Moshammer, J. Phys. B **38**, S753 (2005).
[7] M. Y. Kuchiev, JETP Lett. **45**, 404 (1987).
[8] P. B. Corkum, Phys. Rev. Lett. **71**, 1994 (1993).
[9] K. J. LaGattuta, and J. S. Cohen, J. Phys. B **31**, 5281 (1998).
[10] R. Kopold, W. Becker, H. Rottke, and W. Sandner, Phys. Rev. Lett. **85**, 3781 (2000).
[11] B. Feuerstein, R. Moshammer, D. Fischer, A. Dorn, C. D. Schröter, J. Deipenwisch, J. R. Crespo Lopez-Urrutia, C. Höhr, P. Neumayer, J. Ullrich, H. Rottke, C. Trump, M. Wittmann, G. Korn, and W. Sandner, Phys. Rev. Lett. **87**, 043003 (2001).
[12] G. L. Yudin and M. Y. Ivanov, Phys. Rev. A **63**, 033404 (2001).
[13] H. Sakai, J. J. Larsen, I. Wendt-Larsen, J. Olesen, P. B. Corkum, and H. Stapelfeldt, Phys. Rev. A **67**, 063404 (2003).
[14] A. Staudte, C. L. Cocke, M. H. Prior, A. Belkacem, C. Ray, H. W. Chong, T. E. Glover, R. W. Schoenlein, and U. Saalmann, Phys. Rev. A **65**, 020703(R) (2002).
[15] S. F. L. Larochelle, A. Talebpour, and S. L. Chin, J. Phys. B **31**, 1201 (1998).
[16] H. Niikura, F. Légaré, R. Hasbani, A. D. Bandrauk, M. Yu. Ivanov, D. M. Villeneuve, and P. B. Corkum, Nature (London) **417**, 917 (2002).
[17] D. Zeidler, A. Staudte, A. B. Bardon, D. M. Villeneuve, R. Dörner, and P. B. Corkum, Phys. Rev. Lett. **95**, 203003 (2005).
[18] J. Wu, H. Zeng, and C. Guo, Phys. Rev. A **75**, 043402 (2007).
[19] J. Parker, K. T. Taylor, C. W. Clark, and S. Blodgett-Ford, J. Phys. B **29**, L33 (1996).
[20] D. Dundas, K. T. Taylor, J. S. Parker, and E. S. Smyth, J. Phys. B **32**, L231 (1999).
[21] J. S. Parker, B. J. S. Doherty, K. T. Taylor, K. D. Schultz, C. I. Blaga, and L. F. DiMauro, Phys. Rev. Lett. **96**, 133001 (2006).
[22] R. Grobe and J. H. Eberly, Phys. Rev. Lett. **68**, 2905 (1992).
[23] M. Lein, E. K. U. Gross, and V. Engel, Phys. Rev. Lett. **85**, 4707 (2000).
[24] R. Panfili, S. L. Haan, and J. H. Eberly, Phys. Rev. Lett. **89**, 113001 (2002).
[25] C. Ruiz, L. Plaja, and L. Roso, Phys. Rev. Lett. **94**, 063002 (2005).
[26] C. Ruiz, L. Plaja, L. Roso, and A. Becker, Phys. Rev. Lett. **96**, 053001 (2006).
[27] J. S. Prauzner-Bechcicki, K. Sacha, B. Eckhardt, and J. Zakrzewski, Phys. Rev. Lett. **98**, 203002 (2007).
[28] A. Becker and F. H. M. Faisal, J. Phys. B **29**, L197 (1996).
[29] A. Becker and F. H. M. Faisal, Phys. Rev. Lett. **84**, 3546 (2000).
[30] S. V. Popruzhenko and S. V. Goreslavskii, J. Phys. B **34**, L239 (2001).
[31] A. Becker and F. H. M. Faisal, Phys. Rev. Lett. **89**, 193003 (2002).
[32] C. Figueira de Morisson Faria, X. Liu, W. Becker, and H. Schomerus, Phys. Rev. A **69**, 021402(R) (2004).
[33] C. Figueira de Morisson Faria, H. Schomerus, X. Liu, and W. Becker, Phys. Rev. A **69**, 043405(R) (2004).
[34] J. Chen, J. Liu, L. B. Fu, and W. M. Zheng, Phys. Rev. A **63**, 011404(R) (2000).
[35] K. Sacha and B. Eckhardt, Phys. Rev. A **63**, 043414 (2001).
[36] K. Sacha and B. Eckhardt, Phys. Rev. A **64**, 053401 (2001).
[37] K. T. Taylor, J. S. Parker, D. Dundas, and K. J. Meharg, J. Mod. Opt. **54**, 1959 (2007).
[38] J. S. Prauzner-Bechcicki, K. Sacha, B. Eckhardt, and J. Zakrzewski, Phys. Rev. A **71**, 033407 (2005).
[39] J. Liu, D. F. Ye, J. Chen, and X. Liu, Phys. Rev. Lett. **99**, 013003 (2007).
[40] J. Chen, J. Fan, Y. Li, and S. P. Yang, Phys. Rev. A **76**, 013418 (2007).
[41] Y. Li, J. Chen, S. P. Yang, and J. Liu, Phys. Rev. A **76**, 023401 (2007).
[42] S. Baier, C. Ruiz, L. Plaja, and A. Becker, Phys. Rev. A **74**, 033405 (2006).
[43] S. Baier, C. Ruiz, L. Plaja, and A. Becker, Laser Phys. **17**, 358 (2007).
[44] S. Saugout, C. Cornaggia, A. Suzor-Weiner, and E. Charron, Phys. Rev. Lett. **98**, 253003 (2007).
[45] J. Javanainen, J. H. Eberly, and Q. Su, Phys. Rev. A **38**, 3430 (1988).
[46] A. D. Bandrauk and H. Z. Lu, Phys. Rev. A **72**, 023408 (2005).
[47] A. D. Bandrauk and H. Lu, J. Phys. B **38**, 2529 (2005).
[48] W. Kolos and L. Wolniewicz, J. Chem. Phys. **43**, 2429 (1965).

[49] G. Lagmago Kamta and A. D. Bandrauk, Phys. Rev. A **74**, 033415 (2006).

[50] I. V. Litvinyuk, K. F. Lee, P. W. Dooley, D. M. Rayner, D. M. Villeneuve, and P. B. Corkum, Phys. Rev. Lett. **90**, 233003 (2003).

[51] A. Jaroń-Becker, A. Becker, and F. H. M. Faisal, Phys. Rev. A **69**, 023410 (2004).

[52] A. S. Alnaser, T. Osipov, E. P. Benis, A. Wech, B. Shan, C. L. Cocke, X.-M. Tong, and C.-D. Lin, Phys. Rev. Lett. **91**, 163002 (2003).